

Logic could be learned from images

Qian Guo^{a,c}, Yuhua Qian^{*a,b,c}, Xinyan Liang^{a,c}, Yanhong She^d, Deyu Li^{b,c}, Jiye Liang^{b,c}

^a*Institute of Big Data Science and Industry, Shanxi University, Taiyuan 030006, Shanxi, China*

^b*Key Laboratory of Computational Intelligence and Chinese Information Processing of Ministry of Education, Shanxi University, Taiyuan 030006, Shanxi, China*

^c*School of Computer and Information Technology, Shanxi University, Taiyuan 030006, Shanxi, China*

^d*College of Science, Xi'an Shiyou University, Xi'an 710065, Shaan'xi, China*

Abstract

Logic reasoning is a significant ability of human intelligence and also an important task in artificial intelligence. The existing logic reasoning methods, quite often, need to design some reasoning patterns beforehand. This has led to an interesting question: can logic reasoning patterns be directly learned from given data? The problem is termed as a data concept logic (DCL). In this study, a learning logic task from images, just a LiLi task, first is proposed. This task is to learn and reason the relation between two input images and one output image, without presetting any reasoning patterns. As a preliminary exploration, we design six LiLi data sets (Bitwise And, Bitwise Or, Bitwise Xor, Addition, Subtraction and Multiplication), in which each image is embedded with a n -digit number. It is worth noting that a learning model beforehand does not know the meaning of the n -digit number embedded in images and relation between the input images and the output image. In order to tackle the task, in this work we use many typical neural network models and produce fruitful results. However, these models have the poor performances on the difficult logic task. For furthermore addressing this task, a novel network framework called a divide and conquer model (DCM) by adding some prior information is designed, achieving a high testing accuracy.

Keywords: logic reasoning, data concept logic, LiLi task, reasoning patterns

2010 MSC: 00-01, 99-00

1. Introduction

Human intelligence integrates cognitive functions such as perception, learning, memory, problem solving and logic reasoning [1]. Among them, logic reasoning is a significant ability of human intelligence. Applying the reasoning, humans obtain some rules hidden in complex phenomenon, and even forecast the unknown events. One of the goals of artificial intelligence is to mimic human cognitive functions to the utmost. As a part of cognitive functions, logic reasoning is also an important task in artificial intelligence [2].

Many logic reasoning methods such as fuzzy reasoning [3, 4, 5, 6], FCA [7, 8, 9], probabilistic reasoning [10, 11, 12, 13], evidential reasoning [14, 15, 16], Bayesian reasoning [17, 18] and rough reasoning [19, 20, 21, 22], have been proposed. However, quite often, these methods need to design some reasoning patterns beforehand. For example, in the FCA, one first obtains a formal context applying the domain expert knowledge, then computes the concept lattice from the formal context, and finally achieves knowledge reasoning using the disjunction and conjunction operations. This process not only costs a large amount of time, but also heavily depends on the domain expert experience. But, without mastering special domain knowledge beforehand, human still can directly reason from given data. For example, without mastering knowledge of 3D reconstruction beforehand, people can reconstruct 3D model of an unseen 2D image in his mind through observing and reasoning many 2D images and corresponding 3D scenes in real world. This has led to an interesting research topic: can machine directly learn logic reasoning patterns from given data? And these logic patterns are termed as the data concept logic (DCL).

*Corresponding author.

Email addresses: czguoqian@163.com (Qian Guo), jinchengqyh@126.com (Yuhua Qian), liangxinyan48@163.com (Xinyan Liang), yanhongshe@gmail.com, yanhongshe@xsyu.edu.cn (Yanhong She), lidy@sxu.edu.cn (Deyu Li), ljj@sxu.edu.cn (Jiye Liang)

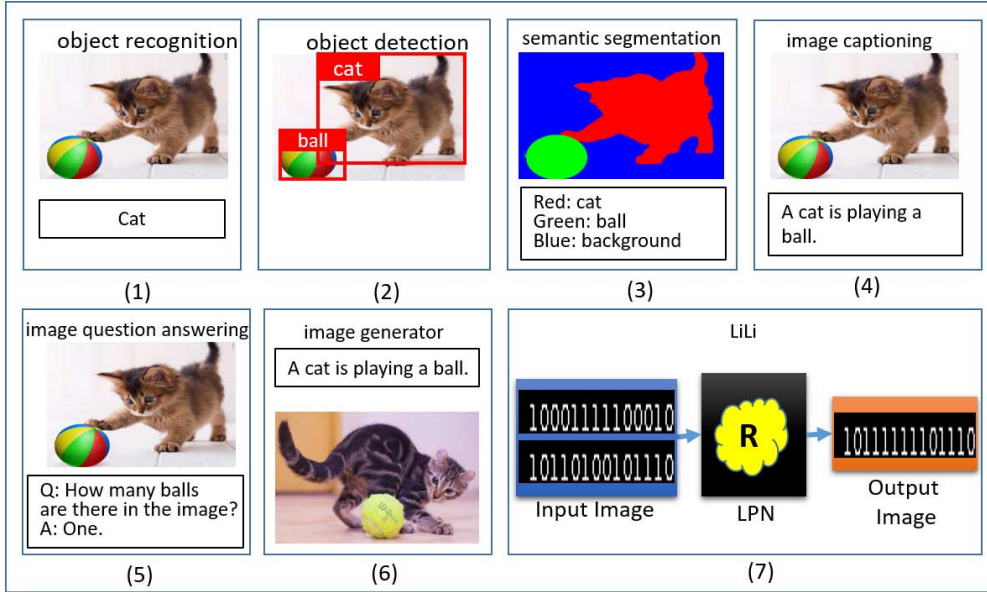


Figure 1: The differences among six popular computer vision tasks (1) Object recognition (sometimes object classification) is to classify individual objects. (2) Object detection is to classify individual objects and localize each using a bounding box. (3) Semantic segmentation is to classify each pixel into a fixed set of categories without differentiating object instances. (4) Image captioning is to describe the content of an image by using reasonably formed natural sentences. (5) Visual question answering (VQA) is to automatically answer natural language questions according to related the image content. (6) Image generator is to generate images according to images or text description. (7) Data concept logic is to learn to obtain logic concepts from a given data set.

As a preliminary exploration, in this study, we design a task of the DCL which is called learning logic task from images, just a LiLi task shown in Fig. 1(7). Unlike the logic operation defined by human (LOH) using some domain expert knowledge, a LiLi task is to learn and reason the relation between two input images and one output image without any reasoning patterns beforehand, i.e. LPN does not know any reasoning patterns about R . In summary, there are some differences below between a LiLi task and a LOH.

- For LiLi, one does not know any reasoning patterns about R except for giving a data set, while for LOH whose focus is that how to define a reasonable logic operation, one always possesses lots of domain knowledge about R .
- LPN induced by a LiLi models an abstract or low level logic relation in term of the pixel values. However, the existing logic operation models a semantic or high level logic relation in term of the numbers or symbols.
- LPN induced by a LiLi is a data-driven method to model the logic relation, while LOH is an expert-driven method.

Learning logic task from images (LiLi task) is also a very important computer vision task. Unfortunately, to the best of our knowledge, there are only a bit of work on the LiLi task shown in Fig. 1(7). In contrast, a variety of models based on deep convolutional neural networks (CNNs) have achieved the state-of-the-art performances, even super-human on some tasks for the common computer vision tasks such as object recognition [23, 24], object detection [25, 26], semantic segmentation [27, 28], image captioning [29, 30], visual question answering (VQA)[31, 32], image generator [33, 34] (see Fig. 1). It is well known that the logic reasoning is one of the abilities that the general/strong artificial intelligence has to possess. In the existing computer vision tasks, image captioning and visual question answering seem to need some reasoning abilities, especially VQA (indeed VQA performs need more knowledge: image itself, common sense, domain knowledge, and so on). In fact, because of strong biases of existing benchmark data sets for VQA, the

systems can correctly answer the questions without reasoning [2, 35, 36]. Hence, it is desired to provide a new task, such as the LiLi tasks, to test the reasoning ability of models.

Our contributions are as follows:

1. The data concept logic (DCL) is proposed to directly learn the concept logic patterns from the given data.
2. We propose a LiLi task where the abstract or low logic relation between two input images and one output image needs to be learned and reasoned without any reasoning patterns beforehand.
3. We provide an inference form of LiLi tasks that is consistent with classical propositional calculus form.
4. Six LiLi task data sets with three difficulty levels: **Bitwise And**, **Bitwise Or**, **Bitwise Xor**, **Addition**, **Subtraction and Multiplication**, are provided.
5. Unlike a semantic or high level logic relation defined by human, an abstract or low level logic relation is expressed by a novel data-driven method called as LPN.
6. The performances of these typical neural networks: LSTM, CNN-LSTM, MLP, CNN-MLP, Autoencoder and ResNets, are tested on six LiLi tasks.
7. The DCM is proposed using a decomposing strategy to solve the difficult task **Multiplication**, achieving a better performance than the typical neural networks used in this paper.

The remainder of this paper is organized as follows: Section 2 proposes the DCL. Section 3 proposes six LiLi data sets, the LiLi tasks and its inference form. Section 4 presents the performance evaluation of the typical neural networks on six LiLi data sets. In Section 5, the DCM is devised to solve the difficult logic task **Multiplication**. Finally, we draw conclusions in Section 6.

2. DCL

In this section, we first detail the DCL proposed in this paper, and then provide an inference form of DCL.

2.1. DCL

Data concept logic (DCL) is a data-driven tool for learning to obtain logic concepts from a given data set directly. Applying the learned concepts, it can output the logic relations among the input data. It is noted that DCL merely uses pure original data cues, and can not know other information such as the meaning of symbols/numbers in data in advance. The DCL can be formalized as follows.

Definition 1. A data concept logic is termed as a triple $\mathcal{R} = (I, R, O)$, where $I = \{x_i \mid x_i = (x_i^1, x_i^2, \dots, x_i^{m_i}), i = 1, 2, \dots, N\}$ is an input sequence with the length m_i , $O = \{y_i \mid y_i = (y_i^1, y_i^2, \dots, y_i^{m_o}), i = 1, 2, \dots, N\}$ is an output sequence with the length m_o , $R : I \rightarrow O$ is a relation mapping from the input I to the output O .

The aim of DCL is to learn a relation mapping R from the input I to the output O . In this paper, we propose a deep learning network framework: Logic Pattern Network (LPN) parameterized by W to learn a logic relation mapping R . This model can be learned by solving the following optimization problem.

$$\begin{aligned} W^* &= \arg \min_W \mathcal{L}(LPN_W(I), O) \\ &= \arg \min_W \frac{1}{N} \sum_{i=1}^N \mathcal{L}(LPN_W(x_i), y_i), \end{aligned} \quad (1)$$

where \mathcal{L} is a loss function, and N is the number of the training samples.

The workflow of a DCL task is illustrated in Fig. 2, where I is the set of input data, O is the set of ground-truth output data, \hat{O} indicates the set of logic relation patterns reasoned by $f(LP_N(x_i^1, x_i^2, \dots, x_i^{j_o}))$, O/I is the ground-truth logic relation set for a given input set I , \hat{O}/I is the prediction logic relation set for a given input set I using LPN, Loss is used to evaluate the difference between O/I and \hat{O}/I . LPN indicates the logical pattern network.

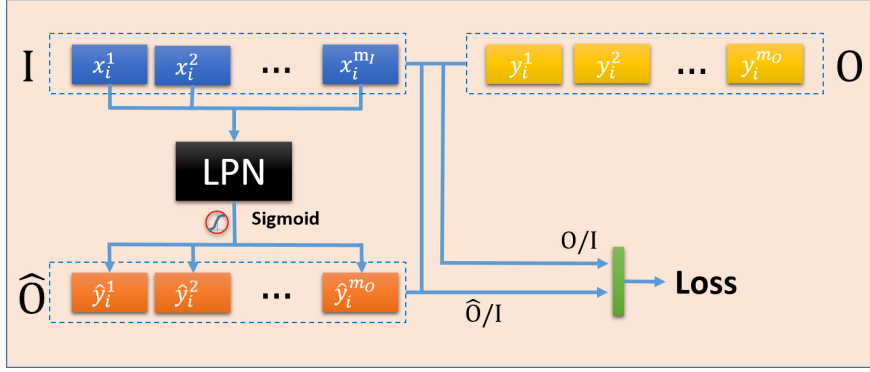


Figure 2: The workflow of a DCL task.

2.2. Inference form of DCL

Human, in our daily life, often makes inferences using some known antecedents. And this process can be formalized as the following form [4].

$$\begin{array}{lcl}
 \text{Antecedent 1 :} & A_1 & \longrightarrow B_1 \\
 \text{Antecedent 2 :} & A_2 & \longrightarrow B_2 \\
 & \vdots & \vdots \\
 \text{Antecedent } n : & A_n & \longrightarrow B_n \\
 \text{Antecedent * :} & A_* & \\
 \hline
 \text{Consequence :} & & B_*
 \end{array} \tag{2}$$

Formula 2 exactly is also the mathematical model of the classical propositional calculus [4] where the consequence of the antecedent * is inferred using the known n antecedents. There exist many methods addressing the task. For example, Zadeh [37] provided an inference rule called ‘compositional rule of inference’ (CRI) to make such an inference whose antecedents and consequences contain fuzzy concepts. Specially, an implication $A \rightarrow B$ first is translated into a fuzzy relation $R_\zeta(A, B)$ from A to B . And then, B_* can be inferred by the composition of R_ζ and A_* by the following formula.

$$B_* = R_\zeta(A, B) \circ A_*, \tag{3}$$

where $R_\zeta : [0, 1]^2 \rightarrow [0, 1]$ defined beforehand by the human experts is a duality function. \circ denotes a composition operator.

Inspired by fuzzy reasoning [4], a DCL task can be written as the following inference form based on the IF THEN

rule.

$$\begin{array}{ll}
\text{Antecedent 1 :} & \text{If the input sequence are } x_1^1, x_1^2, \dots, \text{ and } x_1^{m_i} \text{ then the output sequence is } y_1^1, y_1^2, \dots, \text{ and } y_1^{m_o} \\
\text{Antecedent 2 :} & \text{If the input sequence are } x_2^1, x_2^2, \dots, \text{ and } x_2^{m_i} \text{ then the output sequence is } y_2^1, y_2^2, \dots, \text{ and } y_2^{m_o} \\
& \vdots \\
& \vdots \\
\text{Antecedent } n : & \text{If the input sequence are } x_n^1, x_n^2, \dots, \text{ and } x_n^{m_i} \text{ then the output sequence is } y_n^1, y_n^2, \dots, \text{ and } y_n^{m_o} \\
\text{Antecedent } n + 1 : & \text{If the input sequence are } x_{n+1}^1, x_{n+1}^2, \dots, \text{ and } x_{n+1}^{m_i} \\
\text{Antecedent } n + 2 : & \text{If the input sequence are } x_{n+2}^1, x_{n+2}^2, \dots, \text{ and } x_{n+2}^{m_i} \\
& \vdots \\
& \vdots \\
\text{Antecedent } n + m : & \text{If the input sequence are } x_{n+m}^1, x_{n+m}^2, \dots, \text{ and } x_{n+m}^{m_i} \\
\hline
\text{Consequence } n + 1 : & \text{The output sequence is } y_{n+1}^1, y_{n+1}^2, \dots, \text{ and } y_{n+1}^{m_o} \\
\text{Consequence } n + 2 : & \text{The output sequence is } y_{n+2}^1, y_{n+2}^2, \dots, \text{ and } y_{n+2}^{m_o} \\
& \vdots \\
& \vdots \\
\text{Consequence } n + m : & \text{The output sequence is } y_{n+m}^1, y_{n+m}^2, \dots, \text{ and } y_{n+m}^{m_o}
\end{array} \tag{4}$$

where x_i^1, x_i^2, \dots and $x_i^{m_i}$ are the input data fed into the LPN, y_i^1, y_i^2, \dots and $y_i^{m_o}$ are the output data expressing the relation among the input data.

In formula 4, the n antecedents from 1 to n constituting the training set are used to train the LPN inference model. And the n antecedents from $n + 1$ to $n + m$ constituting the testing set are used to test the inference ability of LPN. Based on this, formula 4 can be further simplified as the following form.

$$\begin{array}{ll}
\text{Training antecedent :} & \begin{array}{l} (x_1^1, x_1^2, \dots, x_1^{m_i}) \longrightarrow (y_1^1, y_1^2, \dots, y_1^{m_o}) \\ (x_2^1, x_2^2, \dots, x_2^{m_i}) \longrightarrow (y_2^1, y_2^2, \dots, y_2^{m_o}) \\ \vdots \\ (x_n^1, x_n^2, \dots, x_n^{m_i}) \longrightarrow (y_n^1, y_n^2, \dots, y_n^{m_o}) \end{array} \\
\text{Testing antecedent :} & \begin{array}{l} (x_{n+1}^1, x_{n+1}^2, \dots, x_{n+1}^{m_i}) \\ (x_{n+2}^1, x_{n+2}^2, \dots, x_{n+2}^{m_i}) \\ \vdots \\ (x_{n+m}^1, x_{n+m}^2, \dots, x_{n+m}^{m_i}) \end{array} \\
\hline
\text{Consequence :} & \begin{array}{l} (y_{n+1}^1, y_{n+1}^2, \dots, y_{n+1}^{m_o}) \\ (y_{n+2}^1, y_{n+2}^2, \dots, y_{n+2}^{m_o}) \\ \vdots \\ (y_{n+m}^1, y_{n+m}^2, \dots, y_{n+m}^{m_o}) \end{array}
\end{array} \tag{5}$$

Formula 5 can be further simplified as the following form by $I_{train} = \{(x_1^1, x_1^2, \dots, x_1^{m_i}), (x_2^1, x_2^2, \dots, x_2^{m_i}), \dots, (x_n^1, x_n^2, \dots, x_n^{m_i})\}$, $O_{train} = \{(y_1^1, y_1^2, \dots, y_1^{m_o}), (y_2^1, y_2^2, \dots, y_2^{m_o}), \dots, (y_n^1, y_n^2, \dots, y_n^{m_o})\}$, $I_{test} = \{(x_{n+1}^1, x_{n+1}^2, \dots, x_{n+1}^{m_i}), (x_{n+2}^1, x_{n+2}^2, \dots, x_{n+2}^{m_i}), \dots, (x_{n+m}^1, x_{n+m}^2, \dots, x_{n+m}^{m_i})\}$, and $O_{test} = \{(y_{n+1}^1, y_{n+1}^2, \dots, y_{n+1}^{m_o}), (y_{n+2}^1, y_{n+2}^2, \dots, y_{n+2}^{m_o}), \dots, (y_{n+m}^1, y_{n+m}^2, \dots, y_{n+m}^{m_o})\}$

$$\begin{array}{ll}
\text{Training antecedent set :} & I_{train} \longrightarrow O_{train} \\
\text{Testing antecedent set :} & I_{test} \\
\hline
\text{Consequence set :} & O_{test}
\end{array} \tag{6}$$

In fact, formula 6 contains three implications, i.e. $(I_{train} \rightarrow O_{train}) \rightarrow (I_{test} \rightarrow O_{test})$. One can obtain the consequence O_{test} of the antecedent I_{test} by translating three implications to the following form.

$$O_{test} = R(I_{train}, O_{train}) \circ I_{test}, \tag{7}$$

where $R(I_{train}, O_{train})$ learnt using a data-driven method is a high-dimension function.

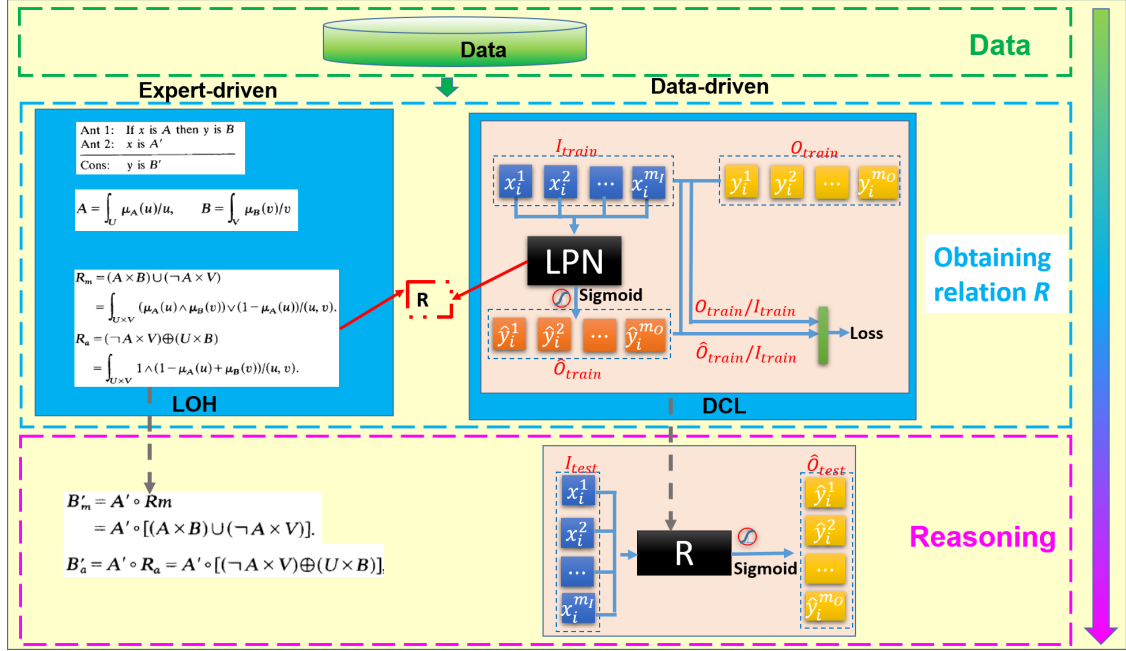


Figure 3: The comparative analysis between the DCL and the LOH.

From the above analysis, one can find that the DCL have the consistent inference form with the classical propositional calculus. The comparison of the DCL and the LOH is illustrated in Fig. 3. From Fig. 3, one can see that one fundamental task of DCL or LOH is obtaining the relation R . For this task, they have a very obvious difference: for LOH, R needs to be defined beforehand by the experts, while for DCL, R is learnt from a given data set.

Based on the above analysis, it is desired to design a human-free and data-driven method directly learn the reasoning pattern from given data. In this study, we explore this problem by proposing the LiLi task. What follows, the LiLi task will be detailed and formalized.

3. A LiLi task

In this section, we first construct six LiLi data sets, then detail the LiLi tasks proposed in this paper, and finally provide its inference form consistent with the classical propositional calculus form.

3.1. LiLi data sets

We first construct six LiLi data sets by embedding the known logic relations in images in this paper to verify the performance of the proposed LPN model.

It is well known that there are numerous known and unknown logic relations in the world. In this paper, these logic relations: **Bitwise And**, **Bitwise Or**, **Bitwise Xor**, **Addition**, **Subtraction** and **Multiplication** are selected to construct these LiLi data sets. It is worth noting that the LPN model does not know the logic relation hidden in images beforehand. Each logic relation consists of 10,000 training samples, 10,000 validation samples and 20,000 testing samples. These testing samples are not included in the training samples or validation samples. In addition, the bitwise operations are binary numbers and arithmetic operations are decimals. For **Bitwise And**, **Bitwise Or** and **Bitwise Xor** data sets, the size of the images is set to 15×120 , so the number embedded in one image is at most a 14-digit number. For **Addition**, **Subtraction** and **Multiplication** data sets, the size of the images is set to 15×60 , hence the number embedded in one image is at most a 7-digit number. This step ensures that the proportion of numbers used for training is a very small fraction of all possible combinations. Each of these samples consists of two input images each containing an integer

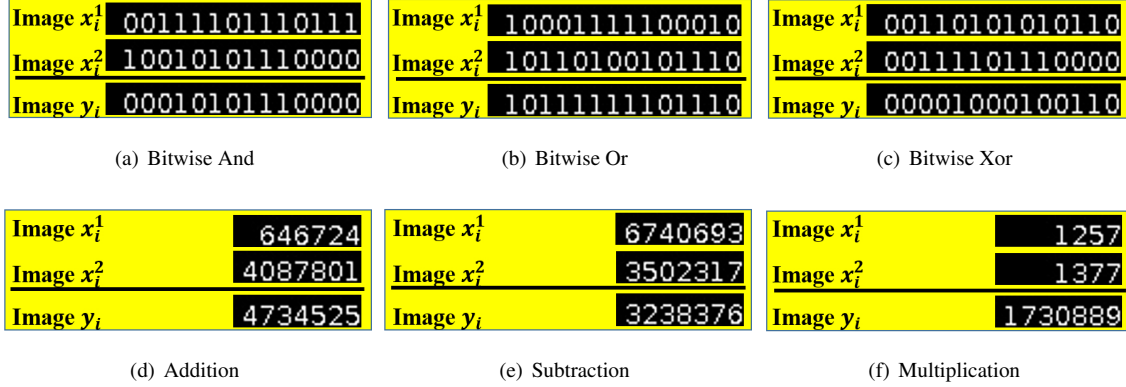


Figure 4: The samples of six LiLi data sets.

number. The pair of two input images marked x_i^1 and x_i^2 are then generated from a pre-specified range as detailed below. The output image marked y_i is generated according to the result of the operation on the two input images. The numbers embedded in images x_i^1 , x_i^2 and y_i are A , B and E .

The details about these data sets are here:

- **Bitwise And:** For per sample, both A and B have 14 binary digits. E is the bitwise *and* of A and B . For example, A and B are “00111101110111” and “10010101110000”, respectively. So, E is “00010101110000”. The sample is shown in Fig. 4(a).
- **Bitwise Or:** For per sample, both A and B have 14 binary digits. E is the bitwise *or* of A and B . For example, A and B are “10001111100010” and “10110100101110”, respectively. So, E is “10111111011110”. The sample is shown in Fig. 4(b).
- **Bitwise Xor:** For per sample, both A and B have 14 binary digits. E is the bitwise *xor* of A and B . For example, A and B are “00110101010110” and “00111101110000”, respectively. So, E is “00001000100110”. The sample is shown in Fig. 4(c).
- **Addition:** For per sample, the range of A and B are 0~4999999. E is the sum of A and B . For example, A and B are “646724” and “4087801”, respectively. So, E is “4734525”. The sample is shown in Fig. 4(d).
- **Subtraction:** For per sample, the range of A and B are 0~9999999. E is the difference between A and B . In order to ensure a positive result, A is chosen to be larger or equal to B . For example, A and B are “6740693” and “3502317”, respectively. So, E is “3238376”. The sample is shown in Fig. 4(e).
- **Multiplication:** For per sample, the range of A and B are 0~3160. E is the product of A and B . For example, A and B are “1257” and “1377”, respectively. So, E is “1730889”. The sample is shown in Fig. 4(f).

According to the difficulty of the logic learning tasks, these data sets are divided into 3 levels: one-star(★, easy), two-star(★★, intermediate), and three-star(★★★, difficult).

Bitwise And, Bitwise Or and Bitwise Xor data sets (★): (1) The value of each digit of E is only determined by the values at the same position in A and B , e.g., in Fig. 4(a), the value at 2^{th} (the rightmost position is 1^{th}) position in E is only determined by the values at 2^{th} position in A and B , so the value at 2^{th} position in E is “0” ($1 \& 0 = 0$); (2) The possible value of each digit of E is 0 or 1.

Addition and Subtraction data sets (★★): (1) The value of each digit of E is determined by the carry or borrow and the values at the same position in A and B , e.g., in Fig. 4(d), the value at 2^{th} position in E is determined by the carry of the sum of values at 1^{th} position in A and B and the values at 2^{th} position in A and B ; (2) The possible value of carry or borrow part is 0 or 1, so the possible value of each digit (except the rightmost position) of E has two possibilities in

0~9, we choose one of the two possibilities as the final result based on the carry case. E.g., in Fig. 4(d), the carry of the sum of values at 1^{th} position in A and B is “0”, the sum of values at 2^{th} position in A and B is “2” ($2+0=2$), so the value at 2^{th} position in E is “2” ($0+2=2$).

Multiplication data set (★★★): (1) The value at a given position of E is determined by the values at the given positions in A and B and all positions in A and B before that given position. E.g., in Fig. 4(f), the value at 2^{th} position in E is determined by the values at 1^{th} and 2^{th} positions in A and the values at 1^{th} and 2^{th} positions in B . (2) The number of the possible value of each digit (except the rightmost position) of the E on **Multiplication** data set is more than that on **Addition or Subtraction** data sets.

3.2. LiLi tasks

In this paper, we focus on the scene where a model directly learns and reasons the relation between two input images and one output image (the output image expresses the relation between two input images), without any reasoning patterns beforehand. In this task, we first generate three images, two for the input and one for the output. The output image expresses the relation between two input images. In addition, the n-digit number embedded in the images are not explicitly introduced, which means that the meaning of contents embedded in images and the relation between two input images and one output image are not known at all. One example is used to illustrate the LiLi task. If the n-digit numbers embedded in two input images are “234” and “432”, the output image are “666”, the logic relation between two input images and the output image is addition. It can be formalized as follows.

Given a data concept logic system as a set of triple $\mathcal{R} = (I, R, O)$, where $I = \{x_i \mid x_i = (x_i^1, x_i^2), i = 1, 2, \dots, N\}$ is an input sequence, $O = \{y_i\}_{i=1}^N$ is the output, where x_i^1, x_i^2 and y_i are three image with K pixels shown in Fig. 4. R denotes the logic relation between the pair of images $x_i \in I$ and $y_i \in O$.

At the semantic or high level, R is called as *Bitwise And*, *Bitwise Or*, *Bitwise Xor*, *Addition*, *Subtraction* and *Multiplication* denoted as $\&$, $|$, \wedge , $+$, $-$ or \times , and they are easily understood by human beings. However, at the abstract or low level, R may be a high-dimensional mapping that is extremely difficult to define the mapping by human, in this paper, $R : [-1, 1]^{2K} \rightarrow \{0, 1\}^K$. Hence, it is desired to design a novel method to express an abstract or low level logic relation.

In this task, given a data set $D = \{(x_i, y_i)\}_{i=1}^N$, where y_i denotes the logic relation between the pair of images x_i^1 and x_i^2 . When drawing these images, we use the pixel value 0 for black, the pixel value 1 for white. For the input images, we scale every pixel value into $-1 \sim 1$ by subtracting the mean, so $x_i^1, x_i^2 \in [-1, 1]^K$. For the output image $y_i \in \{0, 1\}^K$. This task can be viewed as finding a mapping from the input space $I = \{x_i\}_{i=1}^N$ to the output space $O = \{y_i\}_{i=1}^N$ by a supervised learning strategy. In this study, this task can be transformed into a regression problem with the Mean Square Error (MSE) loss function, i.e. \mathcal{L} is *MES*. It can be by solving the following optimization problem.

$$\begin{aligned}
W^* &= \arg \min_W MSE(f(LPN_W(I)), O) \\
&= \arg \min_W \frac{1}{N} \sum_{i=1}^N MSE(f(LPN_W(x_i^1, x_i^2)), y_i) \\
&= \arg \min_W \frac{1}{N} \sum_{i=1}^N \sqrt{\sum_{k=1}^K (f(LPN_W(x_i^1, x_i^2))_k - y_{ik})^2},
\end{aligned} \tag{8}$$

where f is a sigmoid function to transform $LPN_W(x_i^1, x_i^2)$ to $[0, 1]$, i.e. $f(LPN_W(x_i^1, x_i^2)) \in [0, 1]^K$, and LPN is parameterized by W . Formula 8 is differentiable with respect to the parameter W , and can be efficiently solved by using the gradient descent method.

Based on above analysis and discussion, we illustrate the workflow of the LiLi tasks shown in Fig. 5, where I is the set of input image data, O is the set of ground-truth output image data, \hat{O} indicates the set of logic relation patterns reasoned by $f(LPN_W(x_i^1, x_i^2))$, O/I is the ground-truth logic relation set for a given input image set I , \hat{O}/I is the prediction logic relation set for a given input image set I using LPN , Loss is used to evaluate the difference between O/I and \hat{O}/I . LPN indicates the logical pattern network, which is implemented in this paper using LSTM, CNN-LSTM, MLP, Autoencoder, ResNet18, ResNet50, ResNet152 and DCM, respectively. More implementation details about LPN see Section 4.1 and 5.

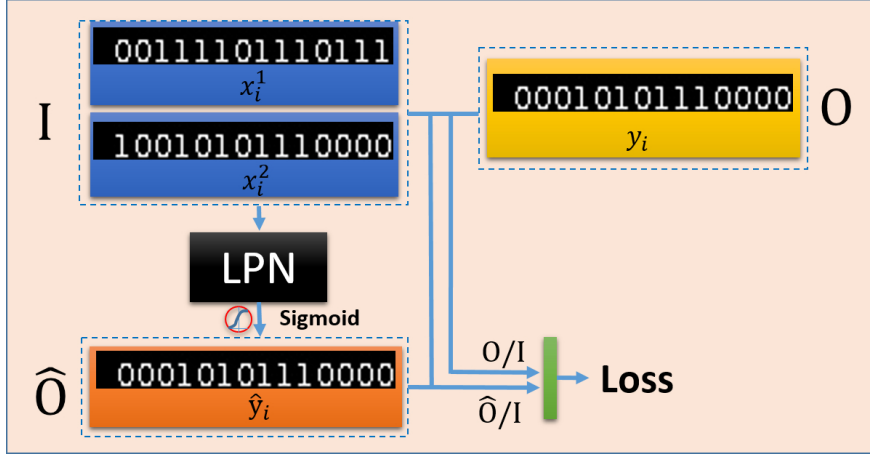


Figure 5: The workflow of a LiLi task.

From formula 8 and Fig. 5, one observes that the LPN merely needs to be provided some training data to automatically learn the logic patterns between a pair of the given images without providing any reasoning patterns beforehand. This is an absolutely data-driven strategy to mine the logic patterns hidden in data.

3.3. Inference form of a LiLi task

Based on the inference form of the DCL 2.2, a LiLi task can be written as the following inference form based on the IF THEN rule.

$$\begin{array}{ll}
 \text{Antecedent 1 :} & \text{If two input images are } x_1^1 \text{ and } x_1^2 \text{ then the output image is } y_1 \\
 \text{Antecedent 2 :} & \text{If two input images are } x_2^1 \text{ and } x_2^2 \text{ then the output image is } y_2 \\
 \vdots & \vdots \\
 \text{Antecedent } n : & \text{If two input images are } x_n^1 \text{ and } x_n^2 \text{ then the output image is } y_n \\
 \text{Antecedent } n + 1 : & \text{If two input images are } x_{n+1}^1 \text{ and } x_{n+1}^2 \\
 \text{Antecedent } n + 2 : & \text{If two input images are } x_{n+2}^1 \text{ and } x_{n+2}^2 \\
 \vdots & \vdots \\
 \text{Antecedent } n + m : & \text{If two input images are } x_{n+m}^1 \text{ and } x_{n+m}^2 \\
 \hline
 \text{Consequence } n + 1 : & \text{The output image is } y_{n+1} \\
 \text{Consequence } n + 2 : & \text{The output image is } y_{n+2} \\
 \vdots & \vdots \\
 \text{Consequence } n + m : & \text{The output image is } y_{n+m},
 \end{array} \tag{9}$$

where x_i^1 and x_i^2 are two images fed into the LPN, y_i is the output image expressing the relation between two input image.

In formula 9, the n antecedents from 1 to n constituting the training set are used to train the LPN inference model. And the n antecedents from $n + 1$ to $n + m$ constituting the testing set are used to test the inference ability of LPN.

Based on this, formula 9 can be further simplified as the following form.

$$\begin{array}{l}
 \text{Training antecedent :} \quad \begin{array}{l} (x_1^1, x_1^2) \longrightarrow y_1 \\ (x_2^1, x_2^2) \longrightarrow y_2 \\ \vdots \\ (x_n^1, x_n^2) \longrightarrow y_n \end{array} \\
 \text{Testing antecedent :} \quad \frac{\begin{array}{l} (x_{n+1}^1, x_{n+1}^2) \\ (x_{n+2}^1, x_{n+2}^2) \\ \vdots \\ (x_{n+m}^1, x_{n+m}^2) \end{array}}{\text{Consequence :}} \quad \begin{array}{l} y_{n+1} \\ y_{n+2} \\ \vdots \\ y_{n+m} \end{array}
 \end{array} \tag{10}$$

Formula 10 can be further simplified as the following form by $I_{train} = \{(x_1^1, x_1^2), (x_2^1, x_2^2), \dots, (x_n^1, x_n^2)\}$, $O_{train} = \{y_1, y_2, \dots, y_n\}$, $I_{test} = \{(x_{n+1}^1, x_{n+1}^2), (x_{n+2}^1, x_{n+2}^2), \dots, (x_{n+m}^1, x_{n+m}^2)\}$, and $O_{test} = \{y_{n+1}, y_{n+2}, \dots, y_{n+m}\}$.

$$\begin{array}{l}
 \text{Training antecedent set :} \quad I_{train} \longrightarrow O_{train} \\
 \text{Testing antecedent set :} \quad I_{test} \\
 \hline
 \text{Consequence set :} \quad O_{test}
 \end{array} \tag{11}$$

One can obtain the consequence O_{test} of the antecedent I_{test} by translating three implications $(I_{train} \rightarrow O_{train}) \rightarrow (I_{test} \rightarrow O_{test})$ included by formula 11 to the following form.

$$O_{test} = R(I_{train}, O_{train}) \circ I_{test}, \tag{12}$$

where $R(I_{train}, O_{train}) : [-1, 1]^{2K} \rightarrow \{0, 1\}^K$ learnt using a data-driven method is a high-dimension mapping function.

According to the above analysis, one can find that on the one hand, the LiLi tasks have the consistent inference form with the classical propositional calculus, on the other hand they have some different aspects as follows.

- $R_z : [0, 1]^2 \rightarrow [0, 1]$ is a duality function. However, $R(I_{train}, O_{train}) : [-1, 1]^{2K} \rightarrow \{0, 1\}^K$ is a complex function with high dimensions (K takes 1800 or 900 in this paper).
- R_z needs to be defined beforehand by the experts, while R is learnt from a given data set because it is almost impossible to define the function beforehand by human.

In real world, there exist many complex relations that can not be provided beforehand by human beings. When facing this situation, the classical propositional calculus can not work well, even cannot work. Hence, it is desired to design a human-free and data-driven method to learn an unknown relation function. This is the our most main motivation.

4. Experiments

In this section, we compare the performances of several typical deep neural networks on the six LiLi tasks. Next, we detail used models and experimental setup.

4.1. Models and experimental setup

For all models, two images as input are fed into the models, and one image as output is used to compare with the ground truth image. These models are trained to produce one output image in which the correct number is embedded by optimising a mean-square error (mse) loss and using the ADAM or SGD optimiser. The early-stopping is used to choose the optimiser and hyper-parameters of smallest loss estimated on the validation set. In addition, the batch size is

Table 1: The hyper-parameter settings on all models.

Model	hyper-parameter
LSTM	LSTM(1024, dropout=0.3)
CNN-LSTM	Conv1(32,(5,5),l2(1.e-4))->BatchNormalization1()->MaxPooling1((2,2))->Conv2(64,(3,3),l2(1.e-4))->BatchNormalization2()->MaxPooling2((2,2))->LSTM(1024, dropout=0.5)
CNN-MLP	Conv1(32,(5,5))->BatchNormalization1()->MaxPooling1((2,2))->Conv2(64,(3,3))->BatchNormalization2()->MaxPooling2((2,2))->Dense1(4096)
MLP	Dense1(256)->Dense2(256)->Dense3(256)
Autoencoder	Conv1(32,(5,5))->MaxPooling1((2,2))->Conv2(64,(5,5))->MaxPooling2((2,2))>Conv3(64,(5,5))->UpSampling1((2,2))->Conv4(32,(5,5))->UpSampling2((2,2))>Cropping2D(((0,1),(0,0)))->Conv5(1,(5,5))

set to 32. The hyper-parameter settings and further details on all models see in Table 1. Finally, the performance values are reported on the testing set.

LSTM and CNN-LSTM: We develop two kinds of models using a standard LSTM module [38] according to the different ways of processing the input images. (1) **LSTM:** Since LSTMs are designed to process inputs sequentially, we first stretch each image into a vector, and then pass each vector sequentially to the LSTM. The final hidden state of the LSTM go through a fully connected layer with sigmoid activation function. The drop-out is applied to the LSTM hidden state. The model achieves the best performance when LSTM hidden layer size is 1024. (2) **CNN-LSTM:** We first pass images sequentially and independently through a 2-layer CNN, and the resulting sequence is handed over to the LSTM. The final hidden state of the LSTM is passed through a fully connected layer with sigmoid activation function. The model is trained using batch normalization after each convolutional layer and drop-out is applied to the LSTM hidden state.

MLP: A fully connected MLP is implemented followed by [39]. The model has three hidden layers each with 256 nodes with ReLU activation functions and one output layer (the same height and width as the input images) with sigmoid activation. All nodes between adjacent layers are fully connected.

CNN-MLP: Inspired by [40], we implement a 2-layer CNN with batch normalization and ReLU activation functions. The input images are treated as a set of separate greyscale input feature maps for the CNN. The convolved output is passed through two-layer, fully connected MLPs, in which the first layer using a ReLU activation function and the second layer using a sigmoid activation function.

Autoencoder: A simple autoencoder network is implemented using the idea of [41]. In this model, a 2-layer CNN is used as the encoder network and a 2-layer upsampling network as the decoder network. At last, a convolutional layer is used as the output layer (the same height and width as the input images) with a sigmoid activation.

ResNet: We use ResNet architecture as described in [42] and modify the softmax activation function to sigmoid activation function on the last layer of the network. In this paper, we train ResNet-18, ResNet-50 and ResNet-152 on all LiLi tasks and get nearly performances.

4.2. Experiments and analysis on LiLi tasks

In this subsection, we test several typical deep neural networks on these LiLi tasks. Each data set consists of 10,000 training samples, 10,000 validation samples and 20,000 testing samples. The testing samples are not included in the training or validation samples. All models are trained on each training set and stopped when the loss on validation set no longer decrease. We use an OCR software [43] to recognize the numbers embedded in the predicted images, and then compare them with the ground truth numbers. For one predicted image, it is right when all digits are equal to the ground truth digits. The accuracies of *Bitwise And*, *Bitwise Or*, *Bitwise Xor*, *Addition*, *Subtraction* and *Multiplication* data sets are shown in Table 2.

From Table 2, one observes that all models get the good performances on *Bitwise And*, *Bitwise Or* and *Bitwise Xor* data sets. Only CNN-MLP, Autoencoder and ResNets get the good performances on *Addition* and *Subtraction* data sets. Unfortunately, all models fail on *Multiplication* data set.

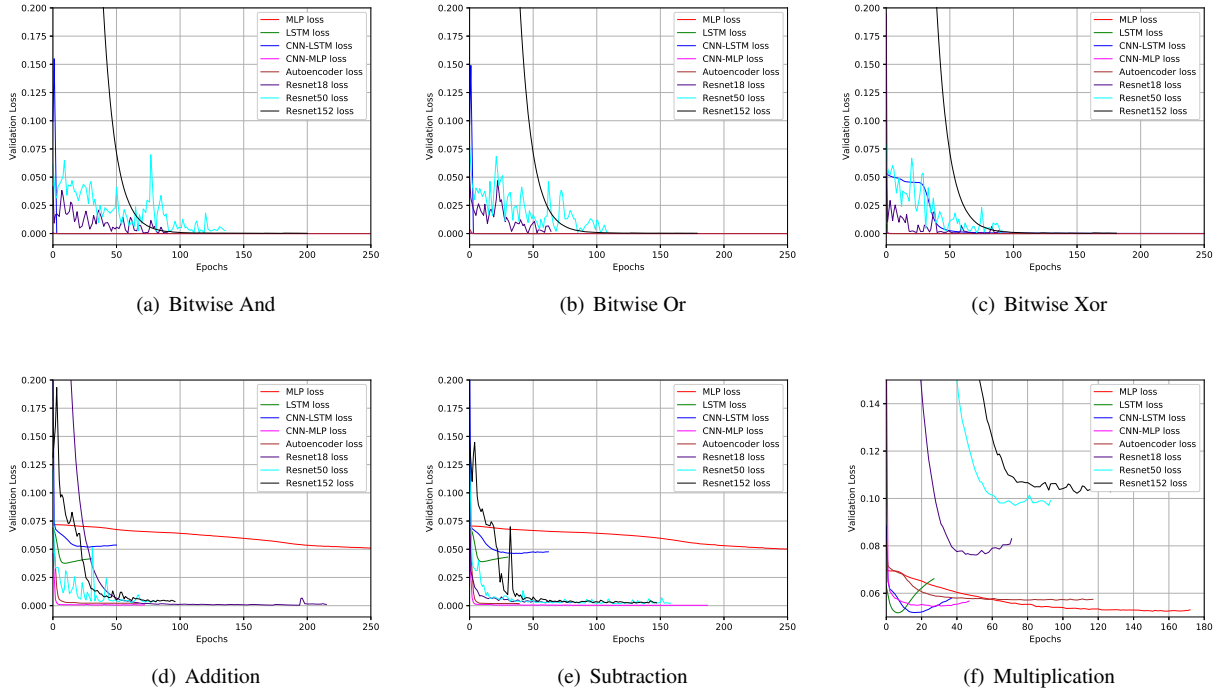


Figure 6: The validation losses of *Bitwise And*, *Bitwise Or*, *Bitwise Xor*, *Addition*, *Subtraction* and *Multiplication* on 10,000 training data sets.

The validation loss curves on *Bitwise And*, *Bitwise Or* and *Bitwise Xor* data sets are shown in Fig.6(a), Fig.6(b) and Fig.6(c). Because of the early-stopping, the epochs of these models are different. From these figures, one finds that all models converge to small losses. In addition, the LSTM, MLP, CNN-MLP and Autoencoder converge faster than the CNN-LSTM and ResNets. The validation loss curves on *Addition and Subtraction* data sets are shown in Fig.6(d) and Fig.6(e). From these figures, one observes that the losses of the CNN-MLP, Autoencoder and ResNets are smaller than other models. Moreover, both of CNN-MLP and Autoencoder converge faster than the ResNets. The validation loss curve on *Multiplication* data set is shown in Fig.6(f). One can see, from it, that all models have very large losses when they converge.

Next, we try to see if increasing data set size could improve model performances. In this scene, all models are trained on 150,000 training data sets and stopped when the loss on validation data sets no longer decreases. The accuracies of all models on six LiLi data sets are shown in Table 3.

From Table 3, one observes that most models get the good performances on *Bitwise And*, *Bitwise Or*, *Bitwise Xor*, *Addition and Subtraction* data sets. It means the performances of models can be improved by increasing the size of data sets. This provides a strategy to solve difficult logic learning problems.

The validation loss curves are shown in Fig.7 on 150,000 training data sets. From Fig.7, one observes that the most of the models converge to smaller losses than before. The validation loss curves on *Bitwise And*, *Bitwise Or* and *Bitwise Xor* data sets are shown in Fig.7(a) to 7(c). From these figures, one finds that the CNN-LSTM and ResNets converge faster than before. The validation loss curves on *Addition*, *Subtraction and Multiplication* data sets are shown in Fig.7(d), Fig.7(e) and Fig.7(f), respectively. From Fig.7(d) and Fig.7(e), one observes that the losses of all models are smaller than before, especially LSTM, CNN-LSTM and MLP. But, from Fig.7(f), we observe that all models still have very large losses when they converge on *Multiplication* data set. A good phenomenon is that the losses of all models are smaller than before.

One guess: the space position plays a significant role in the process of learning logic patterns. It is worth

Table 2: The test accuracies of *Bitwise And*, *Bitwise Or*, *Bitwise Xor*, *Addition*, *Subtraction* and *Multiplication* on 10,000 training data sets.

Model	Operations					
	★			★★		★★★
	Bitwise And	Bitwise Or	Bitwise Xor	Addition	Subtraction	Multiplication
LSTM	100%	100%	100%	0.72%	0.68%	0.09%
CNN-LSTM	100%	100%	100%	0.07%	0.38%	0.10%
MLP	100%	100%	100%	0.21%	0.21%	0.08%
CNN-MLP	100%	100%	100%	96.33%	98.69%	0.07%
Autoencoder	100%	100%	100%	96.78%	97.34%	0.08%
ResNet18	99.96%	98.52%	99.80%	99.86%	99.49%	0.10%
ResNet50	99.92%	99.86%	99.69%	99.14%	99.64%	0.10%
ResNet152	100%	100%	100%	98.74%	98.93%	0.14%

Table 3: The test accuracies of *Bitwise And*, *Bitwise Or*, *Bitwise Xor*, *Addition*, *Subtraction* and *Multiplication* on 150,000 training data sets.

Model	Operations					
	★			★★		★★★
	Bitwise And	Bitwise Or	Bitwise Xor	Addition	Subtraction	Multiplication
LSTM	100%	100%	100%	85.30%	84.06%	0.14%
CNN-LSTM	100%	100%	100%	84.21%	79.22%	0.20%
MLP	100%	100%	100%	98.79%	97.39%	0.16%
CNN-MLP	100%	100%	100%	99.96%	99.96%	0.35%
Autoencoder	100%	100%	100%	98.17%	99.66%	0.16%
ResNet18	100%	100%	100%	99.50%	99.50%	0.24%
ResNet50	100%	100%	100%	99.56%	98.54%	0.26%
ResNet152	99.18%	100%	100%	97.30%	99.68%	0.24%

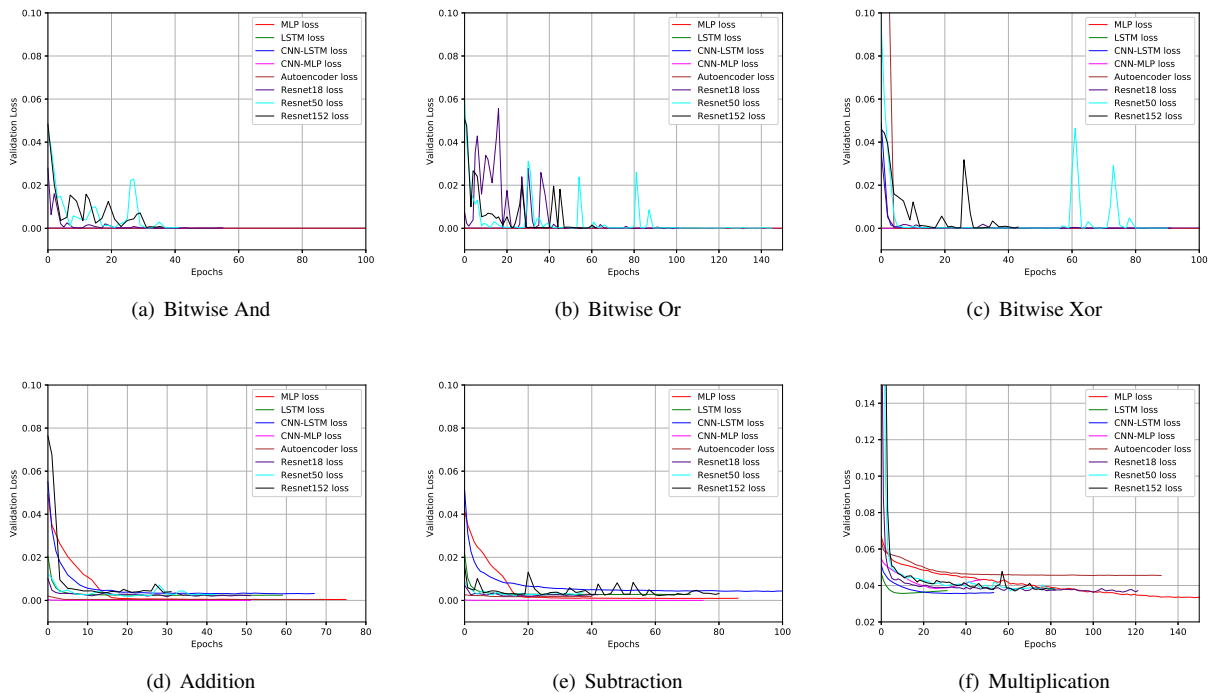
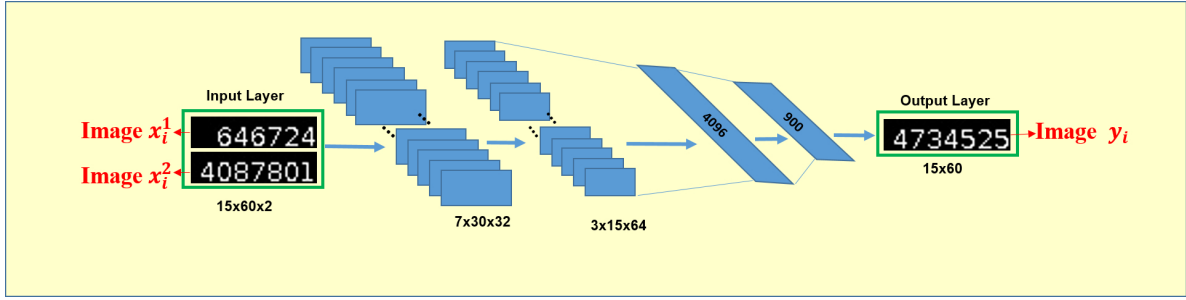


Figure 7: The validation losses of *Bitwise And*, *Bitwise Or*, *Bitwise Xor*, *Addition*, *Subtraction* and *Multiplication* on 150,000 training data sets.

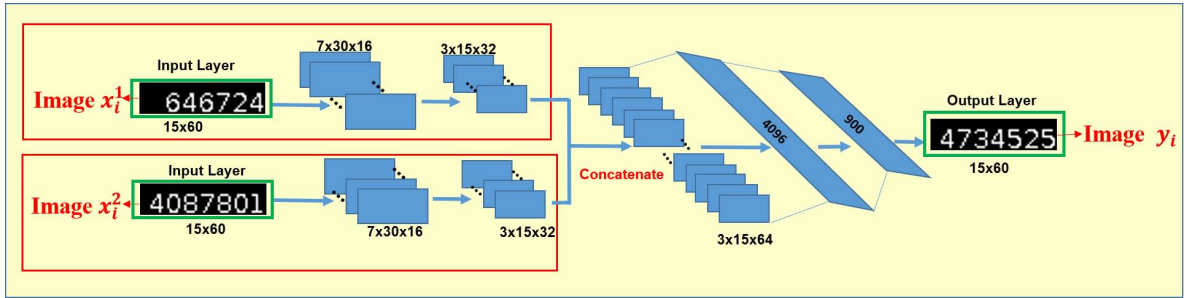
noting that the LSTM and CNN-LSTM only get about 80% accuracies on *Addition* and *Subtraction* data sets even increasing the size of data sets. However, they get 100% accuracies on *Bitwise And*, *Bitwise Or* and *Bitwise Xor* data sets. The reason is that the LSTM and CNN-LSTM are fed the input images one by one, learn the features of the images separately so that they almost do not consider the carry or borrow case on addition or subtraction. Each digit of the result of *addition* and *subtraction* is affected by the adjacent positions (the influences from carry or borrow), while each digit of the result of bitwise and, bitwise or and bitwise xor is not. If the models want to get high accuracies, they should dispose 2 input images a and b simultaneously on *Addition* and *Subtraction* data sets. In order to verify this idea, we develop a model called CNN2-MLP that is similar to CNN-MLP. These two models have same structure and hyper-parameter settings except CNN2-MLP learns features of each of two input images separately. And their structures are shown in Fig.8.

The validation loss curves of CNN-MLP and CNN2-MLP on the six LiLi data sets are shown in Fig. 9. For *Bitwise And*, *Bitwise Or* and *Bitwise Xor* data sets, both of them converge to the small losses. For *Addition* or *Subtraction* data sets, the validation loss of CNN2-MLP is large on 10,000 training data sets. When the size of training data set increasing, the validation loss of CNN2-MLP is smaller than before but still larger than the validation loss of CNN-NLP. For *Multiplication* data set, both of them converge to the large losses. The test accuracies of CNN2-MLP on *Bitwise And*, *Bitwise Or*, *Bitwise Xor*, *Addition*, *Subtraction* and *Multiplication* data sets are shown in Table 4. CNN2-MLP can not get the good performances on *Addition* and *Subtraction* data sets, but still work well on *Bitwise And*, *Bitwise Or* and *Bitwise Xor* data sets. These experiment results verify that the space position plays a significant role in the process of learning logic patterns.

As the size of the given data increases, the MLP tends to have good performances on *Addition* and *Subtraction* data sets. This is because each digit of the result of the addition and subtraction is affected by the adjacent positions in both input images. In particular, for the MLP, the relation between two images at their arbitrary positions, when data set size is small, it can not focus on the exact relation on their adjacent positions. As soon as the data set gets larger, the



(a) CNN-MLP



(b) CNN2-MLP

Figure 8: The architectures of CNN-MLP and CNN2-MLP.

Table 4: The test accuracies of CNN2-MLP on *Bitwise And*, *Bitwise Or*, *Bitwise Xor*, *Addition*, *Subtraction* and *Multiplication* data sets

# training samples	Operations					
	★			★★		★★★
	Bitwise And	Bitwise Or	Bitwise Xor	Addition	Subtraction	Multiplication
150,000	100%	100%	100%	67.47%	62.92%	0.28%
10,000	100%	100%	100%	0.24%	0.20%	0.05%

defect can be made up.

From what has been discussed above, we can divide these models into three categories:

(1) LSTM and CNN-LSTM: These models are appropriate for this type of task where each digit of the result is only affected by the same position of the input numbers (e.g. *Bitwise And*, *Bitwise Or* and *Bitwise Xor* data sets).

(2) MLP: The model is appropriate for this type of task where each digit of the result is affected by all the positions of the input numbers (MLP is more appropriate than other models on *Multiplication* data sets). If the size of data set is large enough, MLP can focus on the same or adjacent positions of the input numbers (e.g. *Bitwise And*, *Bitwise Or*, *Bitwise Xor*, *Addition* and *Subtraction* data sets).

(3) CNN-MLP, Autoencoder and ResNets: These models are appropriate for this type of task where each digit of the result is affected by the same or adjacent positions of the input numbers (e.g. *Bitwise And*, *Bitwise Or*, *Bitwise Xor*, *Addition* and *Subtraction* data sets).

Next, from the standpoint of the visual effects, these models are compared. These predicted results output by the models with the worse performances are shown. For *Addition* and *Subtraction* data sets, only the LSTM, CNN-LSTM and MLP get the poor performances; for *Multiplication* data sets, all models get the poor performances.

For *Addition* and *Subtraction* data sets, the visual effects are shown in Fig.10 and Fig.11. From Fig.10(a) and Fig.11(a), one observes that most models can clearly learn the first and last digits, and other digits obscurely in output

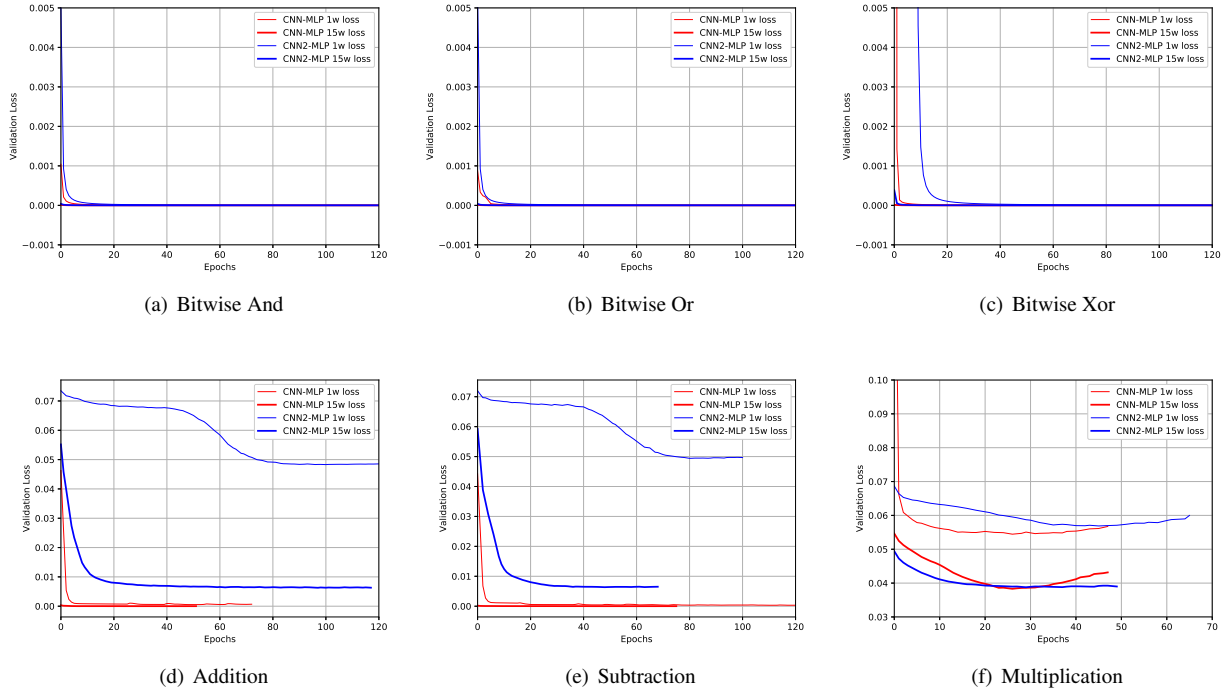


Figure 9: The validation losses of CNN-MLP and CNN2-MLP on *Bitwise And*, *Bitwise Or*, *Bitwise Xor*, *Addition*, *Subtraction* and *Multiplication* data sets.

images. As the size of the training data set increases, from Fig.10(b) and Fig.11(b), one observes that most models can clearly learn most digits in output images. For *Multiplication* data set, the visual effects are shown in Fig.12. From Fig.12(a), we observe that most models can only clearly learn the first and last digits and other digits obscurely in output images. As the size of the training data set increases, from Fig.12(b), one sees that most models can clearly learn more digits than before, but still obscurely for most digits in output images. There are many reasons why the performances of the predicted result on the digits is poor. Some predicted digits are very obscure, e.g. the p_1 is shown in Fig.11(b). Some are similar to other digits, e.g. the p_2 is shown in Fig.10(b). Some are right but OCR can not recognize them, e.g. the p_3 is shown in Fig.11(b). Hence the accuracies can be higher in fact.

From above experimental results, one observes that these models can not solve the difficult LiLi task: *Multiplication*. In the next section, an effective solution is provided by dividing this task into two easier subtasks according to some priori knowledge.

5. Divide and conquer model for *Multiplication* data set

Although increasing the size of data set has effects on solving the difficult logic learning problems, all models still get the poor performances on *Multiplication* data set. To our knowledge, many problems are complex and difficult to solve directly, but it becomes easier when decomposed [44, 45, 46, 47]. Inspired by this, we propose the DCM to address *Multiplication* task adopting the decomposition strategy.

As one sees from Fig.6(f) and Fig.7(f), the MLP is more robust and can converge to a smaller loss than other models. For *Multiplication*, the value at a given position of E is determined by the values at the given position in A and B and all positions in A and B before that given position. MLP is exactly more appropriate this scene than other models. So we select the MLP as the decomposition module of the DCM.

Input Image 1	3309538	842917	2246426	Input Image 1	1962983	1628414	3411343
Input Image 2	2132370	1308754	1084525	Input Image 2	3795605	1429186	687889
Ground Truth	5441908	2151671	3330951	Ground Truth	5758588	3057600	4099232
LSTM	5432908	2252571	3221051	LSTM	5758588	3057600	4099232
CNN-LSTM	5431008	2260571	3201051	CNN-LSTM	5758588	3057600	4099232
MLP	5532908	2061551	3220051	MLP	5758588	3057600	4099232

(a) 10,000 training data set

Input Image 1	1962983	1628414	3411343
Input Image 2	3795605	1429186	687889
Ground Truth	5758588	3057600	4099232
LSTM	5758588	3057600	4099232
CNN-LSTM	5758588	3057600	4099232
MLP	5758588	3057600	4099232

(b) 150,000 training data set

Figure 10: The test visual effects of **Addition** on 10,000 training data set and 150,000 training data set.

Input Image 1	3672080	9042787	3767508	Input Image 1	8030542	6779539	5552176
Input Image 2	2997685	7832285	1157951	Input Image 2	932454	4675453	4885925
Ground Truth	674395	1210502	2609557	Ground Truth	7098088	2104086	666251
LSTM	1638805	2200502	2600657	LSTM	7098088	2104086	666251
CNN-LSTM	1889305	1200502	2609657	CNN-LSTM	7098088	2104086	666251
MLP	526395	1200002	2609557	MLP	7098088	2104086	666251

(a) 10,000 training data set

Input Image 1	8030542	6779539	5552176
Input Image 2	932454	4675453	4885925
Ground Truth	7098088	2104086	666251
LSTM	7098088	2104086	666251
CNN-LSTM	7098088	2104086	666251
MLP	7098088	2104086	666251

(b) 150,000 training data set

Figure 11: The test visual effects of **Subtraction** on 10,000 training data set and 150,000 training data set.

In this experiment, **Multiplication** data set is regenerated by adding some prior information. Each of these samples consists of 4 input images each containing a single integer number. The first two input images are marked a and b , the last two input images are marked c and d . The output image marked e is generated by the result of the multiplication operation on the first two input images. The numbers embedded in images a, b, c, d and e are A, B, C, D and E . For per sample, the ranges of A and B are $0 \sim 3160$. E is the product of A and B . The carry operation occurs when the product of two numbers on one digit is more than ten, and C is used to record the value of carry part, while D is used to record the value of non-carry part. So, the multiplication is divided into the carry part and non-carry part, in other words, the sum of C and D is equal to E . For example, let A and B be “2261” and “584”, respectively, and then, C, D and E equal to “1256300”, “64124” and “1320424”, respectively. The calculation procedure is shown in Fig. 13.

The DCM is divided into three parts: carry part, non-carry part and synthetic part. First, the carry part and non-carry part are used to learn the carries of multiplication and multiplication without carry, respectively. And then, the synthetic part is used to learn the synthetic pattern of the carry part and non-carry part. The network structures of these three parts are similar, but the network parameters are different.

Carry part: During training, the images a and b are used as the input, image c as the ground truth result. The network of the carry part is fully connected and uses the Relu as an activation function in the hidden layers and the sigmoid in the output layer. The carry part has 5 hidden layers, and each layer has 256 units.

Non-carry part: During training, the images a and b are used as the input, the image d as the ground truth result. The network of the non-carry part is fully connected and uses the Relu as an activation function in the hidden layers and the sigmoid in the output layer. The non-carry part has 5 hidden layers, and each layer has 256 units.

Synthetic pattern part: During training, the images c and d are used as the input, the image e as the ground truth result. The network of the synthetic part is fully connected and uses the Relu as an activation function in the hidden layers and the sigmoid in the output layer. The synthetic part has 3 hidden layers, and each layer has 256 units.

The ground truth image is named as x (x can be c, d and e), and the predicted image is named as x' . We hope the number embedded in predicted image e' is equal to the number embedded in ground truth image e , i.e., $E' = E$.

Input Image 1	1721	3113	2618	Input Image 1	2635	1263	358
Input Image 2	2045	2526	1288	Input Image 2	2280	2997	2401
Ground Truth	3519445	7863438	3371984	Ground Truth	6007800	3785211	859558
LSTM	3000005	7000008	3000004	LSTM	5900000	3200011	800058
CNN-LSTM	3000005	7020008	3000004	CNN-LSTM	5900000	3700011	800058
MLP	3000005	2000008	3000004	MLP	5900000	3700011	800058
CNN-MLP	3500005	8020008	3000004	CNN-MLP	6007800	3805011	800058
Autoencoder	3000005	3000008	3000004	Autoencoder	3000000	3000011	1000058
ResNet18	3400445	8000008	3207084	ResNet18	6000000	3700011	800058
ResNet50	3000895	7800578	3000004	ResNet50	6000000	3700011	800058
ResNet152	3500605	7800198	3502684	ResNet152	6000000	3700011	800058

(a) 10,000 training data set

(b) 150,000 training data set

Figure 12: The test visual effects of *Multiplication* on 10,000 training data set and 150,000 training data set.

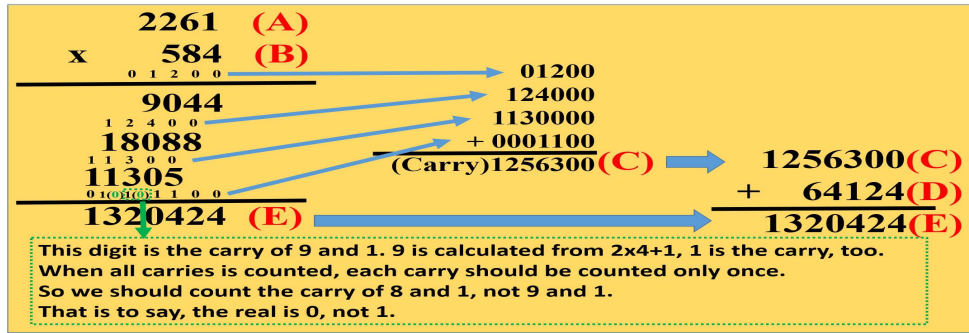


Figure 13: The procedure of multiplication.

Training: During training procedure, the images a and b are used as the input, e as the ground truth result and e' as the output. It is interesting that the images c and d are both the input and ground truth results. For the carry part and non-carry part, the images c and d are the ground truth images, however, for the synthetic part, the image c and d are the input images. Taking the multiplication formula “ $2490 \times 2644 = 6583560$ ” for example explains the training procedure which is shown in Fig. 14(a). A , B , C , D and E are “2490”, “2644”, “2575300”, “4008260” and “6583560”, respectively. The carry part, non-carry part and synthetic part are trained separately. For the carry part and non-carry part, the images a and b are used as the inputs, the images c and d as the ground truth images and the image c' and d' as the outputs, respectively. For the synthetic part, the images c and d are used as input, the image e as the ground truth image and image e' as output. The smaller the differences between predicted image c' , d' and e' as well as ground truth image c , d and e are, the better the performance of DCM is.

Testing: We take the multiplication formula “ $123 \times 124 = 15252$ ” for example to explain the testing procedure which is shown in Fig. 14(b). A and B are “123” and “124”, respectively. In the testing procedure, the DCM only takes images a and b as the input, and then directly gets a predicted image e' at the output end of the synthetic part. E' is “15252” and equals to E which shows that the DCM correctly found the relation between the images a and b only using the pure visual information.

The DCM is trained using the stochastic gradient descent with momentum 0.9, optimising a mean-square error (mse) loss and mini-batch size is fixed 256. The learning rate starts with 0.8, and reduces slowly when the loss plateaus. The training on the carry part, non-carry part and synthetic part terminates when the loss no longer reduces.

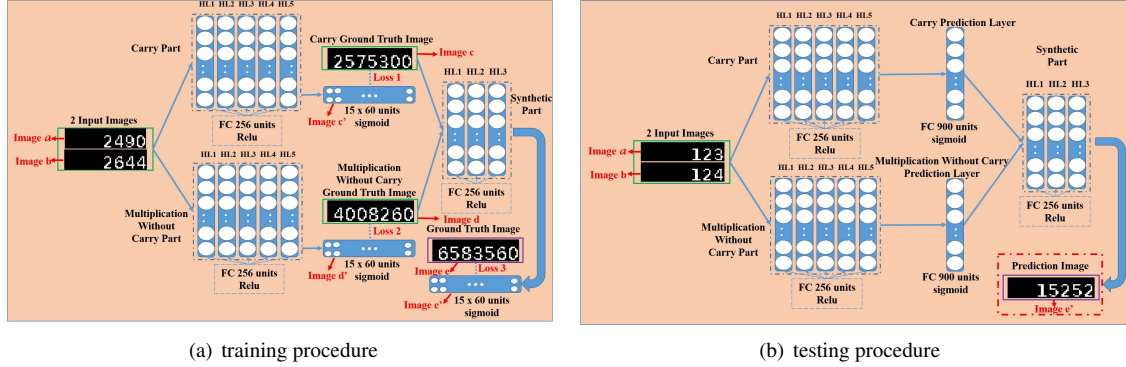


Figure 14: Training and testing procedure.

Table 5: The test accuracy of every part of DCM using 150,000 training examples.

Operation	Network branches		
	Carry part	Operation without carry part	Synthetic pattern part
Multiplication	86.25%	98.38%	84.46%

The accuracy of every part of DCM is shown in Table 5. In contrast, the DCM achieves the surprising accuracy 84.5% which is higher than the MLP on *Multiplication* data set. Some visual effects from the testing are shown in Fig. 15. In Fig. 15(a), both DCM and MLP get correct predicted images. In Fig. 15(b), the DCM gets the correct predicted image, but the MLP does not. In Fig. 15(c), both DCM and MLP predict wrong images. It can be seen that the last two digits and first digit in the image of the MLP are predicted correctly, but the rest central 4 digits are uncertain. However, for the DCM, only one digit of the number embedded in the predicted image is uncertain. That is to say, the DCM can confirm more digits than the MLP.

This owns to the special structure of the DCM. DCM divides a complex task into three simple subtasks, carry part, non-carry part and synthetic part, each subtask only learns one aspect of the task. This helps reducing uncertainty of each predicted digit embedded in the image e' . In order to explain the reason for the effectiveness of the DCM conveniently, we employ some symbols in advance. The goal of the visual logic learning of the arithmetic operations is to compute the value of number 3 in a formula like “number 1 operation number 2 = number 3”. We call the digit of number n at the m^{th} position (the rightmost position is 1^{th}) “ d_n^m ”. The complexity of the task is determined by the level of uncertainty (the amount of possibilities of each digit) in the process of learning logic relation between the input images and output image. For *Addition*, “ d_3^m ” only has two possibilities, “ $(d_1^m + d_2^m) \bmod 10$ ” or “ $(d_1^m + d_2^m + 1) \bmod 10$ ”. The case of “ d_3^m ” on *Subtraction* is similar to addition. However, the uncertainty of multiplication is stronger than that of addition and subtraction, where “ d_3^m ” has ten possibilities.

We assume a formula such as “ $d_1^2 d_1^1 \times d_2^2 d_2^1 = d_3^3 d_3^2 d_3^1$ ” or “ $d_1^2 d_1^1 \times d_2^2 d_2^1 = d_3^3 d_3^2 d_3^1$ ” (if $d_3^4=0$). The scope of each digit “ d_3^m ” (except the digit at rightmost position) is very big, the digit at rightmost position is always a unique and determined value “ $(d_1^1 \times d_2^1) \bmod 10$ ”. The DCM can reduce the uncertainty of predicted number 3. For example, “ d_3^2 ” is determined by the carry and non-carry part during multiplication. In the MLP, the scope of “ d_3^2 ” is 0~9, and the scope of the carry at the 2^{th} position is 0~8. So the carry at the 2^{th} position is to choose one value in 0~8 out of the range 0~9. The non-carry at the 2^{th} position is to choose one value in 0~9. So, there are 900 possibilities ($C_{10}^9 C_9^1 C_{10}^1$) for “ d_3^2 ” in fact. In the MLP, “ d_3^2 ” is directly computed. In contrast, our method is first to compute carry and non-carry respectively, and then synthetic these two parts. The scope of the carry at the 2^{th} position is 0~8, so the carry at the 2^{th} position only needs to determine which one is right in 0~8. The non-carry at the 2^{th} position is to choose one of 0~9. Hence, there are 90 possibilities ($C_9^1 C_{10}^1$) for “ d_3^2 ”. The DCM largely reduces the uncertainty possibilities from 900 to 90. Therefore, the DCM confirms more digits than does the MLP, when the predictions of the two models are all wrong.

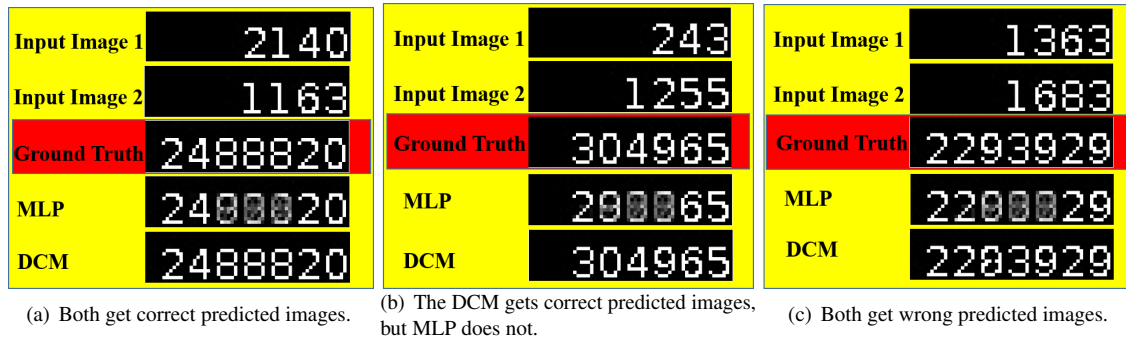


Figure 15: The visual effects of multiplication task on 150,000 training set.

6. Conclusion

In this study, we explore an interesting and important research topic: can logic reasoning patterns be directly learned from given data? As a preliminary exploration, the topic is investigated through a called LiLi task: directly learning from a training image set. In this work, many typical neural network models are used to solve these LiLi tasks and get the good performances on easy and intermediate logic tasks. In order to further solve the difficult task, a new network framework called DCM is developed using a decompose strategy and adding some prior information. This idea can be applied to other complex logic learning tasks. For example, it is difficult to compute decimal bit operation directly, we can convert the decimal to binary first, and then compute binary bit operations. The DCM provides a strategy to solve some difficult logic reasoning tasks combing the domain expert knowledge with data-driven model.

It is a worthy of further study to find more logic reasoning patterns implied in given data. In the future work, there are many important issues to explore for the LiLi tasks, e.g., finding visual functional relations among multiple variables, more complexly logical propositions. More LiLi task data sets containing challenging formulas embedded in the images should be designed.

Acknowledgments

This work was supported by National Key R&D Program of China (No. 2018YFB1004300), National Natural Science Fund of China (No. 61672332, 61322211, 61432011, U1435212, 61502289, 61872226), Program for New Century Excellent Talents in University (No. NCET-12-1031), Program for the Outstanding Innovative Teams of Higher Learning Institutions of Shanxi, Program for the Young San Jin Scholars of Shanxi, and Natural Science Foundation of Shanxi Province (No. 201701D121052).

References

References

- [1] R. Colom, S. Karama, R. E. Jung, R. J. Haier, Human intelligence and brain networks, *Dialogues in clinical neuroscience* 12 (4) (2010) 489.
- [2] J. Johnson, B. Hariharan, L. V. D. Maaten, F. F. Li, C. L. Zitnick, R. Girshick, Clevr: A diagnostic dataset for compositional language and elementary visual reasoning, in: *Proceedings of the IEEE Conference on Computer Vision and Rattern Recognition*, 2017, pp. 1988–1997.
- [3] G. Wang, Fuzzy reasoning and fuzzy logic, in: *Soft Computing in Intelligent Systems and Information Processing. Proceedings of the 1996 Asian Fuzzy Systems Symposium*, 1996, pp. 478–483.
- [4] M. Mizumoto, Comparison of fuzzy reasoning methods, *Fuzzy Sets and Systems* 8 (3) (1982) 253–283.
- [5] J. Yen, Fuzzy logic-a modern perspective, *IEEE Transactions on Knowledge and Data Engineering* 11 (1) (1999) 153–165.
- [6] D. W. Pei, On the strict logic foundation of fuzzy reasoning, *Soft Computing* 8 (8) (2004) 539–545.
- [7] R. Wille, Restructuring lattice theory: an approach based on hierarchies of concepts, in: *Ordered sets*, Springer, 1982, pp. 445–470.
- [8] J. Tadrat, V. Boonjing, P. Pattaraintakorn, A new similarity measure in formal concept analysis for case-based reasoning, *Expert Systems with Applications* 39 (1) (2012) 967–972.
- [9] J. Golinskapilarek, E. Orlowska, Relational reasoning in formal concept analysis, in: *IEEE International Fuzzy Systems Conference*, 2007.

- [10] Y. Yao, Three-way decisions with probabilistic rough sets, *Information Sciences* 180 (3) (2010) 341–353.
- [11] N. J. Nilsson, Probabilistic logic, *Artificial Intelligence* 28 (1) (1986) 71–87.
- [12] N. J. Nilsson, Probabilistic logic revisited, *Artificial Intelligence* 59 (1-2) (1993) 39–42.
- [13] Y. She, X. He, Y. Qian, W. Xu, J. Li, A quantitative approach to reasoning about incomplete knowledge, *Information Sciences* 451-452 (2018) 100–111.
- [14] J. Pearl, Evidential reasoning using stochastic simulation of causal models, *Artificial Intelligence* 32 (2) (1987) 245–257.
- [15] S.-M. Chen, S.-H. Cheng, C.-H. Chiou, Fuzzy multiattribute group decision making based on intuitionistic fuzzy sets and evidential reasoning methodology, *Information Fusion* 27 (2016) 215–227.
- [16] A. Tan, W. Z. Wu, Y. Tao, A unified framework for characterizing rough sets with evidence theory in various approximation spaces, *Information Sciences* 454-455 (2018) S0020025516315900.
- [17] Z. Yang, S. Bonsall, J. Wang, Fuzzy rule-based bayesian reasoning approach for prioritization of failures in fmea, *IEEE Transactions on Reliability* 57 (3) (2008) 517–528.
- [18] J. B. Tenenbaum, T. L. Griffiths, C. Kemp, Theory-based bayesian models of inductive learning and reasoning, *Trends in Cognitive Sciences* 10 (7) (2006) 309–318.
- [19] Y. Qian, X. Liang, W. Qi, J. Liang, L. Bing, A. Skowron, Y. Yao, J. Ma, C. Dang, Local rough set: A solution to rough data analysis in big data, *International Journal of Approximate Reasoning* 97 (2018) 38–63.
- [20] Y. She, X. He, H. Shi, Y. Qian, A multiple-valued logic approach for multigranulation rough set model, *International Journal of Approximate Reasoning* 82 (2017) 270–284.
- [21] Y. Guo, E. C. Tsang, W. Xu, D. Chen, Local logical disjunction double-quantitative rough sets, *Information Sciences* 500 (2019) 87 – 112.
- [22] J. Li, C. Huang, J. Qi, Y. Qian, W. Liu, Three-way cognitive concept learning via multi-granularity, *Information Sciences* 378 (1) (2017) 244–263.
- [23] G. Huang, Z. Liu, L. Van Der Maaten, K. Q. Weinberger, Densely connected convolutional networks, in: *Proceedings of the IEEE Conference on Computer Vision and Pattern Recognition*, 2017, pp. 4700–4708.
- [24] K. He, X. Zhang, S. Ren, J. Sun, Deep residual learning for image recognition, *IEEE Transactions on Pattern Analysis and Machine Intelligence* (2016) 770–778.
- [25] S. Ren, K. He, R. Girshick, J. Sun, Faster r-cnn: Towards real-time object detection with region proposal networks, in: *Advances in Neural Information Processing Systems*, 2015, pp. 91–99.
- [26] K. He, G. Gkioxari, P. Dollár, R. Girshick, Mask r-cnn, in: *Proceedings of the IEEE International Conference on Computer Vision*, 2017, pp. 2961–2969.
- [27] E. Shelhamer, J. Long, T. Darrell, Fully convolutional networks for semantic segmentation, *IEEE Transactions on Pattern Analysis and Machine Intelligence* 39 (4) (2017) 640–651.
- [28] L.-C. Chen, G. Papandreou, I. Kokkinos, K. Murphy, A. L. Yuille, Deeplab: Semantic image segmentation with deep convolutional nets, atrous convolution, and fully connected crfs, *IEEE Transactions on Pattern Analysis and Machine Intelligence* 40 (4) (2018) 834–848.
- [29] O. Vinyals, A. Toshev, S. Bengio, D. Erhan, Show and tell: Lessons learned from the 2015 mscoco image captioning challenge, *IEEE Transactions on Pattern Analysis and Machine Intelligence* 39 (4) (2016) 652–663.
- [30] J. Johnson, A. Karpathy, L. Fei-Fei, Denscap: Fully convolutional localization networks for dense captioning, *IEEE Transactions on Pattern Analysis and Machine Intelligence* (2016) 4565–4574.
- [31] Z. Yang, X. He, J. Gao, L. Deng, A. Smola, Stacked attention networks for image question answering, *IEEE Transactions on Pattern Analysis and Machine Intelligence* (2016) 21–29.
- [32] Q. Wu, C. Shen, P. Wang, A. Dick, A. van den Hengel, Image captioning and visual question answering based on attributes and external knowledge, *IEEE Transactions on Pattern Analysis and Machine Intelligence* 40 (6) (2018) 1367–1381.
- [33] I. Goodfellow, J. Pouget-Abadie, M. Mirza, B. Xu, D. Warde-Farley, S. Ozair, A. Courville, Y. Bengio, Generative adversarial nets, in: *Advances in Neural Information Processing Systems*, 2014, pp. 2672–2680.
- [34] S. Reed, Z. Akata, X. Yan, L. Logeswaran, B. Schiele, H. Lee, Generative adversarial text to image synthesis, in: *International Conference on Machine Learning*, 2016, pp. 1060–1069.
- [35] R. Hu, J. Andreas, M. Rohrbach, T. Darrell, K. Saenko, Learning to reason: End-to-end module networks for visual question answering, in: *Proceedings of the IEEE International Conference on Computer Vision*, 2017, pp. 804–813.
- [36] P. Zhang, Y. Goyal, D. Summers-Stay, D. Batra, D. Parikh, Yin and yang: Balancing and answering binary visual questions, in: *Proceedings of the IEEE Conference on Computer Vision and Pattern Recognition*, 2016, pp. 5014–5022.
- [37] Zadeh, L. A., Outline of a new approach to the analysis of complex systems and decision processes, *IEEE Transactions on Systems, Man and Cybernetics SMC-3* (1) (1973) 28–44.
- [38] A. Graves, Long short-term memory, *Neural Computation* 9 (8) (1997) 1735–1780.
- [39] Y. Hoshen, S. Peleg, Visual learning of arithmetic operation, in: *Association for the Advancement of Artificial Intelligence*, 2016, pp. 3733–3739.
- [40] Y. LeCun, Y. Bengio, G. Hinton, Deep learning, *Nature* 521 (7553) (2015) 436.
- [41] G. E. Hinton, R. R. Salakhutdinov, Reducing the dimensionality of data with neural networks, *Science* 313 (5786) (2006) 504–507.
- [42] K. He, X. Zhang, S. Ren, J. Sun, Deep residual learning for image recognition, in: *Proceedings of the IEEE conference on computer vision and pattern recognition*, 2016, pp. 770–778.
- [43] R. Smith, An overview of the tesseract ocr engine, in: *NICDAR*, Vol. 2, 2007, pp. 629–633.
- [44] Y. Qian, J. Liang, Y. Yao, C. Dang, Mgrs: A multi-granulation rough set, *Information Sciences* 180 (6) (2010) 949–970.
- [45] L. Ke, Q. Zhang, R. Battiti, Hybridization of decomposition and local search for multiobjective optimization, *IEEE Transactions Cybernetics* 44 (10) (2014) 1808–1820.
- [46] J. Liang, J. Fadili, G. Peyré, A multi-step inertial forward-backward splitting method for non-convex optimization, in: *Advances in Neural Information Processing Systems*, 2016, pp. 4035–4043.
- [47] Y. Qian, J. Liang, W. Pedrycz, C. Dang, Positive approximation: An accelerator for attribute reduction in rough set theory, *Artificial Intelligence*

174 (2010) 597–618.